Structure and internal deformation of thrust sheets in the Sawtooth Range, Montana: insights from anisotropy of magnetic susceptibility.

Dave J. McCarthy[1]*, Patrick A. Meere[2] and Michael S. Petronis[3]

[1]British Geological Survey, The Lyell Centre, Edinburgh, EH14 4AP, Scotland

[2]School of Biological, Earth and Environmental Sciences, University College, Cork, Ireland.

[3]Environmental Geology, New Mexico Highlands University, Las Vegas, 87701, New Mexico, USA.

*Corresponding author: davmcc@bgs.ac.uk, tel. +44 131 650 0206

Keywords: AMS, Tectonic Fabrics, Sawtooth Range, Sevier Fold and Thrust Belt

Abstract

Geological strain analysis of sedimentary rocks is commonly carried out using clast-based techniques. In the absence of valid strain markers, it can be difficult to identify the presence of early pre-thrusting/folding tectonic fabric development and resulting Layer Parallel shortening (LPS).

In this contribution, we present results from Anisotropy of Magnetic Susceptibility (AMS) analyses of Mississippian limestones from the Sawtooth Range of Montana. The Sawtooth Range is an arcuate zone of north trending, closely spaced, west dipping, imbricate thrust sheets that place Mississippian Madison Group carbonates above Cretaceous shales and sandstones. This structural regime is a result of the formation of the Cordilleran Mountain Belts of North America. This region is one of the world's classic foreland fold and thrust belts. The degree of deformation increases westward providing an ideal laboratory and geological setting to explore the potential correlation of AMS to thrust related intensity of deformation. The range of magnetic fabrics identified include undeformed bedding controlled depositional fabrics to tectonic fabrics controlled by the regional stress field.

Introduction

The initial formation of a penetrative tectonic fabric or cleavage usually develops as a response to coaxial layer parallel shortening (LPS) in fold and thrust belts (Cooper et al., 1986; Mitra, 1994; Mitra et al., 1985; Yonkee and Weil, 2010). Cleavage formation alone can accommodate up to 60% shortening and develops through a combination of processes, such as pressure solution, grain rotation and grain recrystallisation (Ramsay, 1967 and 1969; Engelder and Marshak, 1985; Passchier and Trouw, 1998).

The Sawtooth Range of North-Western Montana represents the front-range of one of the world's classic fold and thrust belts associated with the deformation and development of the North American Cordillera (Fig. 1). The range is composed of numerous allochthonous thrust sheets of Carboniferous aged carbonates that were parts of the footwall of the regional scale Lewis Eldorado and Hoadley (LEH) Thrust Sheet (Mudge and Earhart, 1980; Mudge, 1972a; Sears, 2001). Despite considerable bulk shortening (~60%), penetrative strain in the Mississippian carbonates has been largely limited to brittle deformation (Holl and Anastasio, 1992), with only a limited development of a penetrative tectonic fabric. In order to determine the extent of the development of this penetrative LPS fabric in the Sawtooth Range, anisotropy of magnetic susceptibility (AMS) data were collected on samples from five thrust sheets; all exposed along the Sun River in the Sawtooth Range (Fig. 2). AMS data are capable of revealing the susceptibility tensor of all the minerals that contribute to the magnetic fabric and lineation of a sample and is, therefore, an ideal method for determining a rock's petrofabric (Borradaile and Jackson, 2004). The Diversion, Sawtooth, French, Norwegian, and Beaver thrust sheets are all well exposed by road cuts and natural outcrops along the Sun River (Fig. 3), allowing good control on sample location within each thrust sheet.

Geological Setting

The central Sawtooth Range is an arcuate zone of predominantly north-south trending, closely spaced, west dipping, imbricate thrust sheets and associated folds comprised of Paleozoic and Mesozoic sedimentary rocks (Fig. 3; Holl and Anastasio, 1992). These eastward propagating thrusts typically placed dominantly Carboniferous Mississippian aged carbonate rocks of the Madison Group above Cretaceous shale and sandstones. Locally Devonian carbonate sequences are also present in the thrust system (Fig. 3; Mudge et al., 1962; Mudge, 1970; DeCelles, 2004).

The interbedded limestones and dolomites of the Madison Group are the most prominent lithologies exposed in the Sun River area (Fig. 3). Underlying the Madison Group Cambrian and Devonian stratigraphic sequence consists predominantly of carbonate rocks, but with subsidiary thin siliciclastic units. Precambrian Belt Supergroup strata consist of marine siliciclastic rocks with subordinate carbonate rock units (Fig. 4; Holl and Anastasio, 1992). The Madison Group is divided into the older Allan Mountain Limestone and the younger Castle Reef Dolomite Formations (Mudge, 1972a). The Allan Mountain Limestone Formation is characterised by thin beds of dark-grey limestone whereas the Castle Reef Dolomite Formation is mostly thick beds of light-grey dolomite (Mudge et al., 1962). These Carboniferous carbonate rocks rest unconformably on Cambrian and Devonian carbonate rocks and are unconformably overlain by Mesozoic strata (Mudge, 1972a). The overlying Mesozoic sequences are composed of Jurassic and Cretaceous marine and non-marine, foreland-basin, mudstone and minor sandstone (Mudge, 1972a).

The thrust sheets typically climb from a basal décollement at the top of the Devonian succession that culminates in the Cretaceous, with minor detachments in the Mississippian Allan Mountain Limestone Formation (Mitra, 1986). Close spacing of thrust surfaces led to the back-rotation and steepening of individual thrust faults in imbricate arrangements, and sigmoidal geometries (Mitra, 1986).

The structural regime and deformation in the Sawtooth Range was generated by the emplacement of the Lewis, Eldorado, and Hoadley (LEH) thrust sheets (Fig. 1; Sears, 2001). The crustal scale LEH thrust package is a large allocthonous sheet composed of siliciclastic Mesoproterozoic to Phanerozoic strata, 70 -110 km wide and up to 30 km thick, with an eastward taper (Sears, 2001). The total displacement on the thrust sheet varies from 40 km to 140 km, with eastward transport initiating at 74 Ma and ceasing by 59 Ma (Sears, 2001; Fuentes et al., 2012). These ages are constrained by disruption in the structural and stratigraphic continuity of Campanian-Maastrichtian volcanogenic formations that are capped by 74 Ma tuffs (Sears, 2001 and references therein) and undeformed porphyritic dykes with an age of 59 Ma that cross cut thrusts at the leading edge of the LEH thrust sheet (Sears, 2001). These age constraints are conformable with direct dating of authigenic clay formation (68-73 Ma) in fault gouge from the Lewis Thrust in SW Canada (van Der Pluijm et al., 2006). The thrust structures exposed in the Sawtooth Range formed as an imbricated thrust wedge in the footwall of the LEH thrust sheet (Sears, 2001).

With the emplacement of the LEH thrust sheet, the strata in the footwall experienced elevated temperature conditions during deformation and imbrication. Maximum temperature conditions have been constrained between 100˚C-175˚C, from illite bearing mineral assemblages recovered from Cretaceous shale (Gill et al., 2002; Hoffman et al., 1976; O’Brien et al., 2006). O’Brien et al. (2006) concluded that chemical remagnetisation associated with these temperature conditions had occurred prior to thrusting and rotation of the carbonate rocks. This thermal regime, largely concurs with vitrinite reflectance studies that suggest only very localised frictional heating associated with large scale thrusting (Bustin, 1983). These data are further interpreted to indicate that any heating associated with the thrust related deformation of the Sawtooth Range did not exceed the temperatures associated with the preceding heating event in the LEH (i.e., 100˚C-175˚C). Holl and Anastasio (1992) estimated that the deformation of the strata of the Sawtooth Range accommodated a minimum bulk shortening of 60% based on section balancing. This shortening was primarily enabled by thrusting associated with the forward developing imbricate fan; thrusting, in turn, was facilitated by progressive development of mesoscopic fault arrays that allowed the base of the thrust sheets to deform by cataclastic flow (Holl and Anastasio, 1992). Tectonic fabrics, were developed, are consistently at a high angle to bedding, and are limited to stylolitisation and spaced cleavage dominated by pressure solution (Fig. 5). This is clearly suggestive of an early (pre-thrusting) localised LPS fabric developed during progressive deformation.

AMS Sampling and Methodology

Oriented block samples were collected from the Madison Group Limestone along the Sun River Valley in a transect arranged from east to west and parallel to the direction of thrust transport. Samples were collected from outcrops with well-defined bedding/cleavage relationships. Lithologies with complex sedimentary fabrics, such as syn-sedimentary deformation, burrowing, and cross bedding were avoided, as these might add further complexities to the relationship between bedding and tectonic fabrics. AMS samples and structural data were obtained from 72 sites. Between 8 and 14 core samples were drilled from each block sample. Out of the 72 block samples collected, 43 block samples survived drilling and yielded enough specimens to be statistically viable (Borradaile and Shortreed, 2011). A minimum of five cylindrical specimens (22 mm × 25 mm) were prepared from each sample, yielding 479 individually oriented specimens for analysis. AMS analyses were carried out using the MFK1-A Kappabridge (AGICO, Czech Republic) at the New Mexico Highlands University Paleomagnetic-Rock Magnetic Laboratory. The MFK1-A Kappabridge has an operating frequency of 976 Hz with an applied field of 200 A/m, and an average sensitivity of ~2.0 × 10−8 SI. Jelinek (1981) statistics were evaluated using Anisoft (version 4.2; AGICO, Czech Republic; Chadima and Jelinek, 2009).

AMS Analysis

Magnetic susceptibility (k) is the induced magnetization (M) that is acquired within an externally applied field (H), k = M/H (Borradaile and Jackson, 2004). The preferred orientation of all magnetic minerals contributes to the observed AMS. Therefore, the total AMS is dependent on the magnetic mineralogy, i.e., the susceptibility and intrinsic anisotropy of minerals and their concentration, as well as their preferred orientation, and in the case of ferromagnetic minerals with a high spontaneous magnetization, their shape and grain size (eg., Tarling and Hrouda, 1993). AMS results are represented by the ellipsoids of magnetic susceptibility, similar to the strain ellipsoid, represented by three mutually orthogonal principal axes K1 ≥ K2 ≥ K3 (Borradaile, 1988, Borradaile & Jackson, 2010). These axes are the eigenvectors and eigenvalues of the bulk susceptibility tensor or Kmean:

$$\bar{K} = \frac{\mathbf{K1} + \mathbf{K2} + \mathbf{K3}}{\mathbf{3}} \qquad \text{(Eqn. 1).}$$

AMS records the net magnetic contribution of all the minerals in a sample, whether they are diamagnetic, paramagnetic, ferrimagnetic (senso stricto), ferromagnetic or anti-ferrimagnetic (Tarling and Hrouda, 1993). Therefore, AMS is dependent on the magnetic (mineral susceptibility and anisotropy) and physical (shape, size, and preferred orientation) properties of these components (Tarling & Hrouda, 1993), and can be representative of all fabrics formed at different times and by different mechanisms.

Consequently, AMS represents a composite fabric which can be related to depositional, diagenetic, magmatic, and tectonic processes, and as a result, fabric interpretation is not always straightforward (e,g., Borradaile and Jackson, 2004). Despite these complications, AMS is typically sensitive to weak tectonic fabrics and their associated slight preferred orientations of minerals, which contribute to the overall magnetic fabric (Aubourg et al., 1991; Averbuch et al., 1992; Borradaile and Tarling, 1981; Fuller, 1963; Kissel et al., 1986; Kligfield et al., 1981; Lowrie et al., 1986; Lüneburg et al., 1999; Parés et al., 1999; Borradaile and Jackson, 2010). It is also important to note that the magnetic ellipsoid, despite accurately representing the rocks petrofabric, cannot be simply correlated with the estimated strain ellipsoid or actual strain. This is due to a number of factors, but not limited to the following: rock composition has a fundamental control on the degree of anisotropy and not strain; the pre-deformation magnetic ellipsoid is not necessarily spherical; and the magnetic ellipsoid may also represent the sum of two competing fabrics, such as primary sedimentary fabrics and cleavage (Hirt et al., 1988 and 1993). Similar problems with non-isotropic original fabrics have been described in traditional strain markers (Dunnet and Siddans, 1971).

A structurally significant magnetic foliation (the plane perpendicular to K3, defined by K1 and K2) and lineation (parallel to K1) can be obtained from this ellipsoid (Borradaile and Jackson, 2004). Additionally, the overall shape of the AMS ellipsoid can be useful for structural interpretations, with three main geometries being oblate (K1 ≅ K2 > K3, with K3 perpendicular to magnetic foliation), prolate (K1 > K2 ≅ K3, with K1 parallel to magnetic lineation) and triaxial (K1 ≠ K2 ≠ K3). In order to quantify and represent these geometries in 2D space the shape and anisotropy parameters of Jelinek (1981) are used. The shape parameter, Tj, is defined as:

$$\mathrm{Tj} = \frac{\left[\mathbf{Ln}\left(\frac{\mathbf{K2}}{\mathbf{K3}}\right) - \mathbf{Ln}\left(\frac{\mathbf{K1}}{\mathbf{K3}}\right)\right]}{\left[\mathbf{Ln}\left(\frac{\mathbf{K2}}{\mathbf{K3}}\right) + \mathbf{Ln}\left(\frac{\mathbf{K1}}{\mathbf{K2}}\right)\right]} \qquad \text{(Eqn. 2).}$$

While the degree of anisotropy, Pj, is defined as:

$$\mathrm{Ln}\left(P_j\right) = \sqrt{2\left(\left(\ln\left(\frac{K1}{K}\right)\right)^2 + \left(\ln\left(\frac{K2}{K}\right)\right)^2 + \left(\ln\left(\frac{K3}{K}\right)\right)^2\right)^{\frac{1}{2}}} \qquad \text{(Eqn. 3).}$$

Tj and Pj can be plotted against each other in Cartesian space (Fig. 6a). Tj values range from −1 (prolate) to +1 (oblate), with a Tj value of 0 representing a triaxial neutral ellipsoid. Pj describes the relative strength of ellipsoid shape anisotropy, with increasing Pj values suggesting a stronger fabric or lineation.

Fabric Types

There is now a considerable amount of work detailing the development of tectonic fabrics in sedimentary rocks with a primary bedding fabric, as observed by AMS (Bakhtari et al., 1998; Graham, 1966; Kligfield *et al*., 1983; Parés *et al*., 1999; Robion *et al*., 1999; Parés, 2004; Burmeister *et al*., 2009). This development can be described using four types of ellipsoid geometries, summarised below and in Figure 6a and b. For a more complete description, see McCarthy *et al*. (2015).

Type 1: An initial sedimentary fabric is typically characterised by a weakly oblate ellipsoid, with slight flattening parallel to bedding. In this case, the K1 and K2 axes are scattered in a girdle representing the magnetic foliation and roughly conforming to bedding, while K3 is perpendicular to the magnetic foliation/bedding. Strong magnetic lineations are rarely present, due to the highly scattered K1.

Type 2: The first sign of an incipient tectonic fabric is typically weaker than the primary sedimentary fabric, therefore the AMS ellipsoid may still be weakly oblate and conformable with bedding. In this case, the K1 axes may start clustering in the direction of extension and defining a magnetic lineation parallel to the intersection of an incipient LPS fabric with bedding.

Type 3: As deformation continues, the magnetic ellipsoid becomes prolate, the K1 axes become strongly clustered and the K2 axes are roughly equal to the K3 axes.

Type 4: The final stage involves a magnetic foliation perpendicular to bedding, with K1 and K2 axes forming a great circle girdle parallel to cleavage. The K1 axes may still be clustered at the intersection of bedding and cleavage, forming a magnetic lineation, or scattered in the plane of cleavage. This stage typically has flattened oblate AMS ellipsoids perpendicular to bedding.

RESULTS

Results from the AMS analyses are presented in Table 1 and summarised in this section. Bulk susceptibility varies from $-3.8X10^{-5}$ SI to $1.9X10^{-4}$ SI, with the majority of samples yielding a negative (diamagnetic) or extremely weak susceptibility (Fig. 7a). Negative and extremely weak positive susceptibilities are common in very pure limestones that lack a volumetrically significant Fe-Ti oxide component or other magnetic Fe-bearing silicate phases. Calcite and dolomite, which are diamagnetic minerals (Hunt et al., 1995), are the dominant carrier of the AMS fabric in samples with negative bulk susceptibilities. The specimens with positive susceptibility values up to $1.9X10^{-4}$ are indicative of minor amounts of paramagnetic minerals, such as phyllosilicates, but these values are at the threshold intensities to indicate the presence of a volumetrically dominant ferromagnetic mineral phase (Rochette, 1987).

The corrected degree of anisotropy (Pj) varies from 1.01 to ~2.00, suggesting a range of fabric strengths, which is comparable to deformed limestones elsewhere (Borradaile et al., 2012). The variation in Pj values do not appear to correlate with changes in bulk susceptibility (Fig. 7a), which implies that Pj is controlled either by primary or tectonic fabrics, rather than the composition of the limestones. Additionally, there is no obvious correlation between the shape parameter (Tj) and bulk susceptibility (Fig. 7b). Pj and Tj values are presented in Figure 8a-e for all specimens in each main thrust sheet. It is evident from these plots that all thrust sheets sampled exhibit a range of AMS ellipsoid geometries from weak oblate through prolate with some samples exhibiting strong oblate geometries.

The contribution of diamagnetic minerals in the sample suite from the Madison Group limestones complicates AMS interpretations. In pure calcite and dolomite, the principal negative susceptibility axis is aligned along the c-axis of the crystal (Borradaile et al., 2012), which is typically perpendicular to schistosity or tectonic cleavage (Flinn, 1965). Therefore, the maximum negative susceptibility axis in diamagnetic materials largely coincides with the normal to the dominant foliation (Borradaile et al., 2012). In order to compare the diamagnetic fabrics to paramagnetic fabrics, the orientation of the maximum (most negative) and minimum (least negative) axes are exchanged (Borradaile et al., 2012).

In an attempt to identify regional magnetic fabrics, specimens have been split into two groups, (A) paramagnetic and (B) diamagnetic, and AMS principle axes plotted on lower hemisphere equal area projections with bedding and cleavage (Fig. 9). These plots show a considerable amount of scatter for both paramagnetic and diamagnetic samples; regardless of being corrected for bedding tilt. There is no clear regional trend for any of the susceptibility axes, but there is some clustering of K1 axes along bedding, cleavage, and the bedding/cleavage intersection lineation.

Interpretation

The AMS fabrics exhibit a range of fabric types that are commonly seen in fold and thrust belts (Bakhtari et al., 1998; Parés, 2004; Weil and Yonkee, 2009; Yonkee and Weil, 2010; McCarthy, 2015). These fabric types evolve from bedding controlled to tectonic cleavage through an intermediate stage with intersecting fabrics (Bakhtari et al., 1998; Borradaile et al., 2012). This evolution of fabric type is evident in the Pj-Tj plots, whereby ellipsoid shapes vary from weakly oblate with flattening parallel to bedding, to prolate with stretching parallel to the extension direction, and a final stage of oblate geometries with flattening perpendicular to bedding (Fig. 10; Parés, 2004). It is interesting to note, that despite this variation in magnetic fabric types, their does not appear to be a regular distribution of bedding controlled versus cleavage controlled fabric types within each thrusts sheet.

Although penetrative tectonic fabrics are poorly developed at an outcrop scale, there is a regular correlation with AMS fabrics and recorded cleavage fabrics at a high angle to bedding, with K1 lineation axes plotting along a cleavage plane or at the cleavage bedding intersection lineation (Fig. 11).

Where penetrative deformation fabrics are observed, they are at a high angle to bedding and largely limited to stylolitisation and occasional spaced cleavage. The poor development of penetrative fabrics in the Madison Limestones may be attributed to the relatively low burial temperature conditions experienced. The temperatures of 100˚C-175˚C constrained by illitic mineral assemblages (Gill et al., 2002; Hoffman et al., 1976; O'Brien et al., 2006) are below the temperatures required (200˚C-300˚C) for intra-crystalline plastic flow of calcite to become a dominant deformation mechanism (Engelder and Marshak, 1985). Analysis of thin sections reveal that grain scale deformation is limited to Type 1 calcite twinning (Ferrill et al., 2004) and grain boundary bulging (Passchier and Trouw, 2005). Both of these textures indicate deformation temperatures below 170°C. The presence of a tectonic stylolitic fabric consistently at a high angle to bedding suggests that this fabric developed prior to thrusting. This is further confirmed by the coaxial folding of stylolites with bedding (Ward and Sears, 2007).

Discussion

The main structures of the Sawtooth Range are characterised by thrust faults that place Madison Limestone over Cretaceous Shale (Holl and Anastasio, 1992). The emplacement of these thrusts was largely enabled by progressive development of mesoscopic fault arrays that allowed the base of the thrust sheets to deform by cataclastic flow (Holl and Anastasio, 1992). This brittle deformation is the most pervasive style of deformation at the base of each thrust sheet, with little or no penetrative deformation present. Therefore, it is argued that the thrust sheets were emplaced in a largely passive manner; with minor penetrative strain.

This is significantly different from the stages of tectonic fabric development during thrust emplacement described by Sanderson (1982), whereby if cleavage developed during thrusting, it would be expected to develop at an oblique angle to bedding (Fig. 12). Similarly, Evans and Dunne (1991) identified four key deformation events associated with thrust sheet evolution: 1) initial Layer Parallel Shortening (LPS); 2) bending and folding at a ramp hinge; 3) syn-thrusting related simple shear; and 4) post-emplacement flattening. These models suggest that LPS development precedes or is synchronous with thrust sheet emplacement, which is then followed by further deformation. Evans and Dunne (1991) also highlighted that the style of penetrative strain recorded in thrust sheets is dependent on whether the right temperature and pressure conditions are present to accommodate grain scale deformation, and that these conditions can vary temporally and spatially within a thrust sheet.

The AMS results presented here do not identify any penetrative deformation that could be linked to syn-thrusting strain. Furthermore, the only penetrative tectonic fabrics identified were consistently perpendicular to bedding and appeared to be of a domainal nature. This is in agreement with the field studies that LPS occurred prior to thrust sheet emplacement.

Therefore, a schematic model for strain evolution in the Sawtooth Range is presented in Figure 12b. The first stage of deformation involves thrust fault initiation and related folding, facilitated by brittle deformation in the hangingwall fault boundary as described by Holl and Anastasio (1991). As this fault develops LPS occurs in the relatively undeformed footwall, which responds by developing an incipient cleavage. Further movement of the thrust fault along the footwall ramp promotes fracturing in structurally competent units such as the Allan Mountain Limestone and Castle Reef Dolomite Formations. With further faulting, the zone of brittle deformation widens and cleavage development continues in the footwall. When deformation transfers further into the foreland, a new thrust fault develops in the footwall and cleavage development ceases as compression is accommodated by a new foreland-ward phase of thrusting. Similar studies in the Wyoming fold and thrust belt that suggested LPS developed in individual thrust sheets prior to thrusting and as a consequence of shortening under the influence of the overriding thrust sheet (Wiltschko and Dorr, 1983).

Conclusion

The carbonate dominated thrust sheets in the Sawtooth Range were emplaced in a largely passive manner. This rotation was facilitated by brittle deformation at the base of the thrust sheets as well as ductile deformation in the Cretaceous strata of the footwalls. The emplacement of these sheets effectively rotated an early or pre-thrusting LPS fabric. Furthermore, no penetrative fabric developed in the carbonates by deformation associated with thrusting has been detected by the AMS analyses.

Acknowledgements

D. McCarthy acknowledges the receipt of an IRCSET Embark scholarship, during which this research was carried out. Graham Leslie and Emrys Philips are thanked for internal reviews and providing discussions that greatly enhanced the manuscript. Richard Allmendinger and Nestor Cardozo are thanked for the use of their Stereonet software (Allmendinger et al., 2013). This paper is published with the permission of the Executive Director of the British Geological Survey (NERC).

References

Allmendinger, R.W., Cardozo, N.C., Fisher, D., 2013. Structural geology algorithms: vectors & tensors: Cambridge. Cambridge University Press, England (289 pp.).

Aubourg, C., Rochette, P., Vialon, P., 1991. Subtle stretching lineation revealed by magnetic fabric of Callovian-Oxfordian black shales (French Alps). Tectonophysics 185, 211–223.

Averbuch, O., Lamotte, D.F. de, Kissel, C., 1992. Magnetic fabric as a structural indicator of the deformation path within a fold-thrust structure: a test case from the Corbières (NE Pyrenees, France). J. Struct. Geol. 14, 461–474.

Bakhtari, H.R., Frizon de Lamotte, D., Aubourg, C., Hassanzadeh, J., 1998. Magnetic fabrics of Tertiary sandstones from the Arc of Fars (Eastern Zagros, Iran). Tectonophysics 284, 299–316.

Borradaile, G., Tarling, D., 1981. The influence of deformation mechanisms on magnetic fabrics in weakly deformed rocks. Tectonophysics 77, 151–168.

Borradaile, G.J., 1988. Magnetic susceptibility, petrofabrics and strain. Tectonophysics, 156(1-2), pp.1-20.

Borradaile, G.J., Jackson, M., 2004. Anisotropy of magnetic susceptibility (AMS): magnetic petrofabrics of deformed rocks. Geol. Soc. London, Spec. Publ. 238, 299–360.

Borradaile, G.J., Jackson, M., 2010. Structural geology, petrofabrics and magnetic fabrics (AMS, AARM, AIRM). J. Struct. Geol. 32, 1519–1551.

Borradaile, G.J., Shortreed, C., 2011. Magnetic fabrics in L–S tectonites: How many specimens? J. Struct. Geol. 33, 481–486.

Borradaile, G., Almqvist, B., Geneviciene, I., 2012. Anisotropy of magnetic susceptibility (AMS) and diamagnetic fabrics in the Durness Limestone, NW Scotland. J. Struct. Geol. 34, 54–60.

Burmeister, K.C., Harrison, M.J., Marshak, S., Ferré, E.C., Bannister, R.A. and Kodama, K.P., 2009. Comparison of Fry strain ellipse and AMS ellipsoid trends to tectonic fabric trends in very low-strain sandstone of the Appalachian fold–thrust belt. Journal of Structural Geology, 31(9), pp.1028-1038.

Bustin, R., 1983. Heating during thrust faulting in the rocky mountains: friction or fiction? Tectonophysics 95, 309–328.

Chadima, M. and Jelinek, V., 2009. Anisoft 4.2: anisotropy data browser for windows. Agico. Inc, Brno.

Cooper, M.A. and Trayner, P.M., 1986. Thrust-surface geometry: implications for thrust-belt evolution and section-balancing techniques. Journal of Structural Geology, 8(3-4), pp.305-312.

DeCelles, P.G., 2004. Late Jurassic to Eocene evolution of the Cordilleran thrust belt and foreland basin system, western U.S.A. Am. J. Sci. 304, 105–168.

DeCelles, P.G. and Coogan, J.C., 2006. Regional structure and kinematic history of the Sevier fold-and-thrust belt, central Utah. Geological Society of America Bulletin, 118(7-8), pp.841-864.

Dunnet, D. and Siddans, A.W.B., 1971. Non-random sedimentary fabrics and their modification by strain. Tectonophysics, 12(4), pp.307-325.

Engelder, T., Marshak, S., 1985. Disjunctive cleavage formed at shallow depths in sedimentary rocks. J. Struct. Geol. 7, 327–343.

Ferrill, D.A., Morris, A.P., Evans, M.A., Burkhard, M., Groshong, R.H. and Onasch, C.M., 2004. Calcite twin morphology: a low-temperature deformation geothermometer. Journal of Structural Geology, 26(8), pp.1521-1529.

Flinn, D., 1965. On the Symmetry Principle and the Deformation Ellipsoid. Geol. Mag. 102, 36–45.

Fuentes, F., DeCelles, P.G. and Constenius, K.N., 2012. Regional structure and kinematic history of the Cordilleran fold-thrust belt in northwestern Montana, USA. *Geosphere*, pp.GES00773-1.

Fuller, M.D., 1963. Magnetic Anisotropy and Paleomagnetism. J. Geophys. Res. 68, 293–309.

Gill, J.J., Elmore, R.R.., Engel, M.. M., 2002. Chemical remagnetization and clay diagenesis: testing the hypothesis in the Cretaceous sedimentary rocks of northwestern Montana. Phys. Chem. Earth, Parts A/B/C 27, 1131–1139.

Graham, J.W., 1966. Significance of magnetic anisotropy in Appalachian sedimentary rocks. The earth beneath the continents, pp.627-648.

Hirt, A.M., Lowrie,W., Clendenen,W.S., Kligfield, R., 1988. The correlation of magnetic anisotropy with strain in the Chelmsford formation of the Sudbury Basin, Ontario. Tectonophysics 145, 177–189.

Hirt, A.M., Lowrie,W., Clendenen,W.S., Kligfield, R., 1993. Correlation of strain and the anisotropy of magnetic susceptibility in the Onaping Formation: evidence for a nearcircular origin of the Sudbury basin. Tectonophysics 225 (4), 231–254.

Hoffman, J., Hower, J., Aronson, J., 1976. Radiometric dating of time of thrusting in the disturbed belt of Montana. Geology 4, 16–20.

Holl, J., Anastasio, D., 1992. Deformation of a foreland carbonate thrust system, Sawtooth Range, Montana. Geol. Soc. Am. … 104, 904–953.

Hunt, C. P., Moskowitz, B. M., and Banerjee, S.K., 1995. Magnetic properties of rocks and minerals. In: Thomas J. Ahrens (ed.) Rock Physics and Phase Relations: a Handbook of Physical Constants, pp. 189 – 204. AGU reference shelf 3.

Jelinek, V., 1981. Characterization of the magnetic fabric of rocks. Tectonophysics, 79(3-4), pp.T63-T67.

Kissel, C., Barrier, E., Laj, C., Lee, T., 1986. Magnetic fabric in “undeformed” marine clays from compressional zones. Tectonics 5, 769–781.

Kligfield, R., Owens, W., Lowrie, W., 1981. Magnetic susceptibility anisotropy, strain, and progressive deformation in Permian sediments from the Maritime Alps (France). Earth Planet. Sci. Lett. 55, 181–189.

Lowrie, W., Hirt, A., Kligfield, R., 1986. Effects of tectonic deformation on the remanent magnetization of rocks. Tectonics 5, 713–722.

Lüneburg, C.M., Lampert, S.A., Lebit, H.D., Hirt, A.M., Casey, M., Lowrie, W., 1999. Magnetic anisotropy, rock fabrics and finite strain in deformed sediments of SW Sardinia (Italy). Tectonophysics 307, 51–74.

McCarthy, D.J., Meere, P.A. and Petronis, M.S., 2015. A comparison of the effectiveness of clast based finite strain analysis techniques to AMS in sandstones from the Sevier Thrust Belt, Wyoming. Tectonophysics, 639, pp.68-81.

Mitra, G., 1994. Strain variation in thrust sheets across the Sevier fold-and-thrust belt (Idaho-Utah-Wyoming): Implications for section restoration and wedge taper evolution. J. Struct. Geol. 16, 585–602.

Mitra, G., Yonkee, W.A., Adolph Yonkee, W., 1985. Relationship of spaced cleavage to folds and thrusts in the Idaho-Utah-Wyoming thrust belt. J. Struct. Geol. 7, 361–373.

Mitra, S., 1986. Duplex structures and imbricate thrust systems: geometry, structural position, and hydrocarbon potential. Am. Assoc. Pet. Geol., Bull.;(United States).

Mudge, M., 1970. Origin of the disturbed belt in northwestern Montana. Geol. Soc. Am. Bull. 81, 377–392.

Mudge, M., 1972a. Pre-Quaternary rocks in the Sun River Canyon area, northwestern Montana.

Mudge, M., 1972b. Structural geology of the Sun River Canyon and adjacent areas, northwestern Montana: US Geol. Surv. Prof. Pap. 52.

Mudge, M., 1982. A resume of the structural geology of the Northern Disturbed Belt, northwestern Montana.

Mudge, M., Earhart, R., 1980. The Lewis thrust fault and related structures in the disturbed belt, northwestern Montana.

Mudge, M., Sando, W., Dutro, JT, J., 1962. Mississippian rocks of Sun River Canyon area, Sawtooth Range, Montana. Assoc. Pet. Geol. Bull.

O'Brien, V.J., Elmore, R.D., Engel, M.H., Evans, M.A., 2006. Origin of orogenic remagnetizations in Mississippian carbonates, Sawtooth Range, Montana. J. Geophys. Res. Earth 112, 297–301.

Pares, J.M., 2004. How deformed are weakly deformed mudrocks? Insights from magnetic anisotropy. Geol. Soc. London, Spec. Publ. 238, 191–203.

Parés, J.M., van der Pluijm, B.A., Dinarès-Turell, J., 1999. Evolution of magnetic fabrics during incipient deformation of mudrocks (Pyrenees, northern Spain). Tectonophysics 307, 1–14.

Passchier, C.W., Trouw, R. a. J., 1998. Microtectonics. Springer Berlin Heidelberg, Berlin, Heidelberg.

Ramsay, J.G., 1967. Folding and fracturing of rocks. McGraw-Hill, New York.

Ramsay, J.G., 1969. The measurement of strain and displacement in orogenic belts. Geological Society, London, Special Publications, 3(1), pp.43-79.

Ramsay, J.G. and Huber, M.I., 1983. Techniques of modern structural geology, Volume 1: Strain analysis.

Robion, P., Averbuch, O. and Sintubin, M., 1999. Fabric development and metamorphic evolution of lower Palaeozoic slaty rocks from the Rocroi massif (French–Belgian Ardennes): new constraints from magnetic fabrics, phyllosilicate preferred orientation and illite crystallinity data. Tectonophysics, 309(1), pp.257-273.

Rochette, P., 1987. Magnetic susceptibility of the rock matrix related to magnetic fabric studies. J. Struct. Geol. 9, 1015–1020.

Sanderson, D., 1982. Models of strain variation in nappes and thrust sheets: a review. Tectonophysics 88, 201–223.

Sears, J.W., 2001. Lewis-Eldorado-Hoadley Thrust Slab in the Northern Montana Cordillera , USA : Implications for steady-state orogenic processes 301, 359–373.

Tarling, D.H., Hrouda, F., 1993. The Magnetic Anisotropy of Rocks. Chapman Hall.

Ward, E., Sears, J., 2007. Reinterpretation of fractures at Swift Reservoir, Rocky Mountain thrust front, Montana: Passage of a Jurassic forebulge? Geol. Soc. Am. Spec. Pap. 433, 197–210.

Weil, A.B., Yonkee, a., 2009. Anisotropy of magnetic susceptibility in weakly deformed red beds from the Wyoming salient, Sevier thrust belt: Relations to layer-parallel shortening and orogenic curvature. Lithosphere 1, 235–256.

Wiltschko, D., Dorr, J., 1983. Timing of deformation in overthrust belt and foreland of Idaho, Wyoming, and Utah. Am. Assoc. Pet. Geol. Bull. 67, 1304–1322.

Wu, S., 1993. Fractal strain distribution and its implications for cross-section balancing. J. Struct. Geol. 15, 1497–1507.

Yonkee, A., Weil, A., 2010. Reconstructing the kinematic evolution of curved mountain belts: Internal strain patterns in the Wyoming salient, Sevier thrust belt, USA. Geol. Soc. Am. ….

Figure Captions

Table 1 Table of AMS parameters.

Figure 1 Regional tectonic map of the North American Cordillera modified from DeCelles and Coogan (2006). The study area is indicated with a heavy rectangle (AOI).

Figure 2 Aerial photograph looking north across the Sawtooth Range by Bobak Ha'Eri (licensed under CC by 3.0), the Gibson Reservoir is in the right foreground and the Sun River extends eastward from the reservoir. Thrust geometries can be clearly seen with consistent westward dips. The section line A-A' shows the approximate location of the cross section in Fig. 3b.

Figure 3 a) Map of the Sun River area (redrawn from Mudge, 1982). **b)** Cross-section of line indicated in above map as A-A' (redrawn from Fuentes et al., 2012).

Figure 4 Stratigraphic succession encountered in the Sawtooth Range (modified from Mudge, 1972a; Holl and Anastasio, 1992; Fuentes et al., 2012).

Figure 5 Field and sample images. **a.** Overview looking north of the frontal thrusts of the Sawtooth Range. Carboniferous age carbonates are thrust over Cretaceous shales. **b.** View looking northeast across Diversion Lake at Home Thrust and the overlying Sawtooth Thrust. **c.** View looking northeast of the Sawtooth thrust sheet from the French Thrust. **d.** Vertical solution seams cross-cutting bedding and running parallel to the hammer handle. Bedding is also vertical in this case, identified by lenses of chert above the hammer. **e.** Stylolitisation perpendicular to a bedding plane in Allan Member Limestone Fm. **f.** Thin section of Allan Mountain Limestone Formation. Field of view is approximately 4 mm. The coarse grained texture while ideal for strain analysis is rarely observed. Microstructural deformation observed is mainly grain boundary bulging and type 1 calcite twinning.

Figure 6 a) The progression in ellipsoid shapes under progressive deformation using a Pj-Tj plot, modified from Parés (2004). Increases in Pj, the degree of anisotropy, imply increasing strength of the ellipsoid shape. Tj represents the shape parameter; positive numbers imply an oblate ellipsoid,whereas negative values imply a prolate ellipsoid, perfectly triaxial ellipsoids are represented by Tj values of 0. The representative fabric block diagrams are from Ramsay and Huber (1983). **b)** The evolution of ellipsoid orientations by progressive deformation (LPS) of an originally horizontal bedding fabric (Type 1). As LPS deformation continues the AMS ellipsoid becomes triaxial and starts to resemble Type 2. The first visible stage of deformation is associated with the development of a lineation (Type 3), typically represented by a prolate ellipsoid. As deformation continues this lineation becomes a foliation (Type 4) that is perpendicular to the original bedding plane. Modified from Bakhtari et al. (1998).

Figure 7 AMS results A. Bulk susceptibility values versus corrected degree of anisotropy (Pj) B. Bulk susceptibility versus shape parameter (Tj).

Figure 8 Pj-Tj plots of samples from each thrust sheet. **a)** Diversion thrust. **b)** Sawtooth thrust. **c)** French thrust. **d)** Norwegian thrust. **e)** Beaver thrust. Interestingly all thrust sheets, with the exception of French, exhibit the same pattern of AMS ellipsoid evolution from weakly oblate to strongly oblate through a prolate stage.

Figure 9 Stereographic projections of principal axes for all specimens separated into two groups, paramagnetic (**a**) and diamagnetic (**b**). Individual bedding planes are indicated and primarily dip to westward. Average cleavage orientation is indicated. The second row shows the same data but corrected for bedding tilt for both paramagnetic (**c**) and diamagnetic (**d**) samples. Hollow symbols represent points plotting in the upper hemisphere.

Figure 10 Enlarged geological map of study area. Sample locations are identified in italics. Stereographic projections of principal susceptibility axes for representative block samples across the sampled thrust sheets are shown. Location of cross section in Figure 11 is indicated.

Figure 11 Stereographic projections of principal susceptibility axes for representative block samples across the sampled thrust sheets. Also shown is the inclination of magnetic foliation relative to bedding and tectonic stylolites. Magnetic fabric types are indicated. Inset illustrates evolution of magnetic fabric types assuming horizontal bedding.

Figure 12 a) Strain development during thrusting (redrawn from Sanderson 1982). Top figure illustrates hypothetical strain ellipsoids during thrusting. Cross-hatching in lower figure shows areas of overprinted strains. **b)** Fault model for the Sawtooth Range (modified from Holl and Anastasio, 1992). The relationship between brittle and rotated penetrative deformation (S1) is illustrated.

Table 1

Anisotropy of Magnetic Susceptibility Data from Rocky Mountain Front																		
SITE		**N**	**K1**	**K2**	**K3**	**Km**	**K1**	***K1 95%***	**K2**	***K2 95%***	**K3**	***K3 95%***	**L**	**F**	**P**	**Pj**	**T**	**U**
							Dec/Inc	***Error***	**Dec/Inc**	***Error***	**Dec/Inc**	***Error***						
Field Block Samples																		
BGR2	Home	12	1.006	0.833	0.514	0.784	253.1/35	*70.1/19.4*	112.9/47.7	*70.2/42.3*	358.4/20.7	*43.3/19.5*	1.207	1.620	1.955	1.997	0.438	0.297
BGR3	Home	11	1.046	1.007	0.947	1.000	80.8/5.1	55.5/19.7	190.9/75.6	55.0/50.4	349.5/13.5	51.3/23.6	1.04	1.064	1.105	1.11	0.249	0.225
BGR4	Home	12	-0.93	-0.98	-1.09	-1.000	213.9/76.3	69/29.7	48.5/18.9	69/27.5	329.7/6.1	48.5/18.9	1.11	1.05	1.165	1.17	-0.35	0.387
BGR5	Home	16	1.183	1.007	0.796	0.995	261.4/58.9	48.2/29.4	16.3/14.3	49.2/32.5	113.8/27	35.5/29.1	1.18	1.264	1.485	1.49	0.184	0.087
Gr3	Home	10	0.472	0.309	0.008	0.263	174.6/.1	*58.3/42.1*	84.4/57.7	*61.8/24.6*	264.6/32.3	*52.6/30.1*	2.069	-3.175	-6.568	0.000	0.000	0.296
BGR6	Home	10	1.004	1.003	0.993	1.000	210.8/28.2	79.0/32	344.6/52.3	79/47.4	107.7/22.9	48.1/32.9	1	1.01	1.011	1.01	0.725	0.724
BGR7	Home	11	-0.96	-1.01	-1.03	-1.000	234.1/11.5	32.9/22	348.4/63.8	51.3/28.6	139.1/23.2	50.4/22	1.03	1.048	1.075	1.08	0.299	-0.03
BGR8	Home	14	-0.94	-1.01	-1.06	-1.000	227.1-12.3	48.5/25.1	101.7/69.3	51.9/41.2	320.8/16.3	47.6/28.4	1.05	1.071	1.125	1.13	0.159	-0.13
Gr8	Home	6	-0.976	-0.978	-1.046	-1.000	281.1/35.4	*71.6/5.1*	138.5/48.2	*71.6/13.9*	25.5/19.3	*16.9/6.3*	1.069	1.003	1.072	1.082	-0.919	0.922
Gr6	Home	16	0.162	0.073	-0.235	0.000	324.1/15	*47.7/9.9*	149.7/74.9	*47.8/16.1*	54.5/1.4	*17.9/9.2*	2.232	-0.309	-0.691	0.000	0.000	0.549
BGR13	Diversion	11	1.014	0.622	0.336	0.657	60.8/20.7	30.1/8.4	202.4/64.3	27.3/18.6	325.1/14.6	27.9/16.7	1.55	1.418	2.198	2.2	-0.11	-0.3
BGR12	Diversion	12	-0.49	-0.7	-0.79	-0.659	79.1/14.9	30.4/12	193.4/57.1	61.7/11.7	340.7/28.6	62.3/22	1.12	1.439	1.618	1.65	0.513	-0.42
BGR11	Diversion	13	-0.94	-1.01	-1.04	-1.000	44.1/12.6	28.4/13.7	149.1/49.4	39.4/27.9	304.1/37.9	39.3/13.3	1.03	1.073	1.107	1.11	0.388	-0.37
BGR10	Diversion	14	-0.97	-0.99	-1.04	-1.000	36.6/16.5	43.8/24.3	163/63.4	44.9/25.3	300.3/20.2	32.9/16.2	1.05	1.028	1.08	1.08	-0.3	0.315
BGR16	Diversion	7	-0.94	-1	-1.06	-1.000	40.7/28	56.4/25.4	272.2/49.5	57.1/21.4	146.2/26.7	28.7/24.7	1.06	1.06	1.012	1.12	0.024	0.004
BGR15	Diversion	10	1.009	0.999	0.992	1.000	241.4/18.4	59.1/28.5	332.4/2.9	67.9/58.6	71.1/71.4	67.8/28	1.01	1.007	1.018	1.02	-0.02	-0.18
BGR14	Diversion	14	1.193	0.726	0.536	0.818	247.7/7.2	33.1/21.2	350.3/60	46.1/32.1	153.7/29	46.2/20.6	1.64	1.356	2.227	2.24	-0.24	-0.42
Gr10	French	13	1.104	0.992	0.863	0.986	276.9/24.2	*37.7/8.2*	169.9/33.1	*50.9/37.6*	35.7/46.9	*51/5.4*	1.112	1.150	1.279	1.280	0.134	0.074
Gr11	French	13	1.071	1.016	0.913	1.000	58/19.8	*20.3/8*	155.7/20.5	*20.5/11.9*	239/15	*13.2/6.2*	1.054	1.113	1.173	1.177	0.341	0.306
Gr12	French	11	1.052	1.024	0.924	1.000	138.6/35	*11.1/2.9*	20.7/33.7	*11.3/3.3*	260.5/37	*4.2/3.7*	1.027	1.108	1.138	1.146	0.583	0.561
Gr13	French	9	-0.966	-1.006	-1.028	-1.000	155.2/6.4	*30.9/15.4*	320.5/83.4	*56.6/26.8*	65/1.7	*56.1/16.5*	1.022	1.042	1.064	1.065	0.308	-0.293
Gr33	French	8	0.828	0.740	0.682	0.750	210/83.5	*27.3/14.7*	338.5/4.1	*49/19.2*	68.9/5.1	*50.5/13*	1.120	1.084	1.214	1.215	-0.017	0.211
Gr37	Norwegian	10	-0.970	-0.990	-1.040	-1.000	156.1/1.7	*37.1/8.3*	252.5/75.3	*36.5/15.1*	65.6/14.6	*15.2/12.4*	1.051	1.020	1.072	1.074	-0.422	0.436
Gr5B	Norwegian	6	-0.133	-0.371	-0.496	-0.333	259.3/26	*15.2/10.2*	145.5/39.6	*39.4/13.6*	12.8/39.3	*39.9/9.3*	1.336	2.790	3.727	3.985	0.560	-0.313
Gr36	Norwegian	16	0.915	0.859	0.851	0.875	183.1/51.1	*10.1/5.9*	32.5/35.1	*59.8/8.4*	291.9/14.6	*59.8/6.5*	1.056	1.009	1.076	1.083	-0.075	0.076
BGR20	Norwegian	13	1.02	1.007	0.973	1.000	248.8/48	34/14.3	65.2/42	33.7/11.7	156.7/1.6	15.8/11	1.01	1.035	1.048	1.05	0.449	0.439
Gr39	Norwegian	12	-0.494	-0.713	-0.957	-0.721	334.4/22.5	*52.1/25.2*	195.1/61.4	*52.3/36.8*	71.6/16.8	*38.4/27*	1.341	1.443	1.936	1.938	0.111	0.052
Gr35	Norwegian	14	-0.768	-0.875	-0.928	-0.857	99.6/39.8	*33.4/15.2*	303.6/47.6	*56/25.4*	200/12.2	*55/17.1*	1.060	1.140	1.210	1.215	0.382	-0.341
BGR19	Norwegian	11	1.035	0.998	0.967	1.000	313.1/19.9	16.7/4.8	202.3/44.5	16.7/5.3	60/38.9	6.3/3.6	1.04	1.031	1.07	1.07	-0.09	-0.11
Gr34	Norwegian	10	1.043	1.004	0.953	1.000	199/43.4	*11.9/4.0*	0.4/45	*11.7/10.3*	100/9.4	*10.4/4.4*	1.038	1.053	1.094	1.094	0.160	0.138
Gr38	Norwegian	8	1.060	1.002	0.938	1.000	316.4/22.5	*26.4/8.7*	204.2/42.5	*26.1/15*	66.1/39.1	*31.2/11.3*	1.058	1.068	1.130	1.130	0.082	0.052
BGR21	Norwegian	17	-0.68	-0.83	-1.13	-0.880	217.8/4.3	59.4/31.4	114/72.4	59.2/50.6	309.1/17	51.1/34	1.36	1.213	1.654	1.66	-0.02	0.347
Gr24	Beaver	9	-0.840	-0.983	-1.177	-1.000	337.5/14.5	*21.9/3.9*	238.9/30.1	*27.1/8.5*	89.9/55.9	*21.8/4.4*	1.198	1.170	1.401	1.402	-0.069	0.152
Gr23	Beaver	8	-0.800	-0.976	-1.158	-0.978	349/20.8	*8.5/1.8*	87.3/20.9	*18.7/8.5*	218.2/59.8	*18.7/1.8*	1.187	1.219	1.447	1.447	0.072	0.020
Gr21	Beaver	15	-0.973	-0.990	-1.036	-1.000	288.1/40.7	*46.3/19.1*	44.2/27.1	*46.3/27.4*	157.2/37.3	*27.9/18.6*	1.047	1.017	1.065	1.067	-0.463	0.475
Gr20	Beaver	10	-0.098	-0.993	-1.025	-0.705	234.3/14.5	*50.4/26.6*	87.9/72.8	*50.8/28.9*	326.7/9.1	*35.4/19.7*	1.032	1.011	1.043	1.045	-0.488	0.496
Gr19	Beaver	8	-0.096	-0.979	-1.061	-0.712	229.4/5.5	*50.5/13.5*	124.7/69.1	*50.3/16.1*	321.4/20.1	*18.9/11.9*	1.084	1.020	1.105	1.112	-0.609	0.625
Gr30	Beaver	7	0.186	0.137	0.106	0.143	115.6/44.4	*9.3/5.3*	13.3/12.2	*12.5/8.4*	271.6/43	*12.7/6.2*	1.362	1.287	1.753	1.754	-0.100	-0.237
Gr32	Beaver	7	-0.958	-0.983	-1.058	-1.000	251.9/1.6	*53.4/8.7*	159.9/50.8	*53.5/11.8*	343.2/39.1	*14.1/6.4*	1.076	1.026	1.104	1.108	-0.481	0.500
Gr25	Beaver	12	-0.955	-0.984	-1.062	-1.000	318.2/19.5	*67.3/45.2*	187/61.8	*67.3/45.2*	55.5/19.6	*49.1/29.7*	1.079	1.030	1.112	1.116	-0.438	0.459
Gr18	Beaver	11	-0.307	-0.431	-0.650	-0.463	128.3/1.5	*19.3/10*	260.2/87.8	*19.6/13.4*	38.3/1.6	*16.6/6.7*	1.508	1.402	2.114	2.116	-0.097	0.278
Gr17	Beaver	9	1.021	0.998	0.981	1.000	129.6/30.5	*21.3/15.5*	35.6/6.8	*46.3/20.1*	294.4/58.6	*46.5/15.5*	1.024	1.017	1.041	1.041	-0.163	-0.172
Gr15	Beaver	15	1.013	1.004	0.983	1.000	317.4/18.4	*40.1/11.7*	158.8/70.3	*40.7/14.9*	49.7/6.7	*17.5/11.7*	1.009	1.022	1.031	1.032	0.439	0.433

Figure

Click here to download Figure Sawtooth figures reduced size.pdf

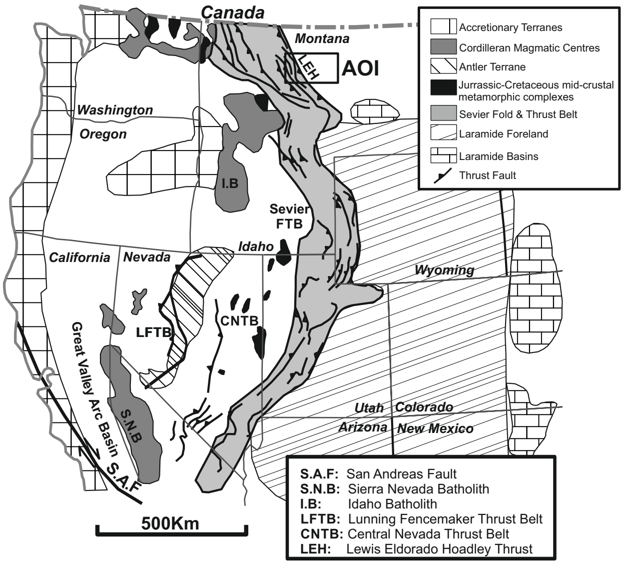

Figure 1

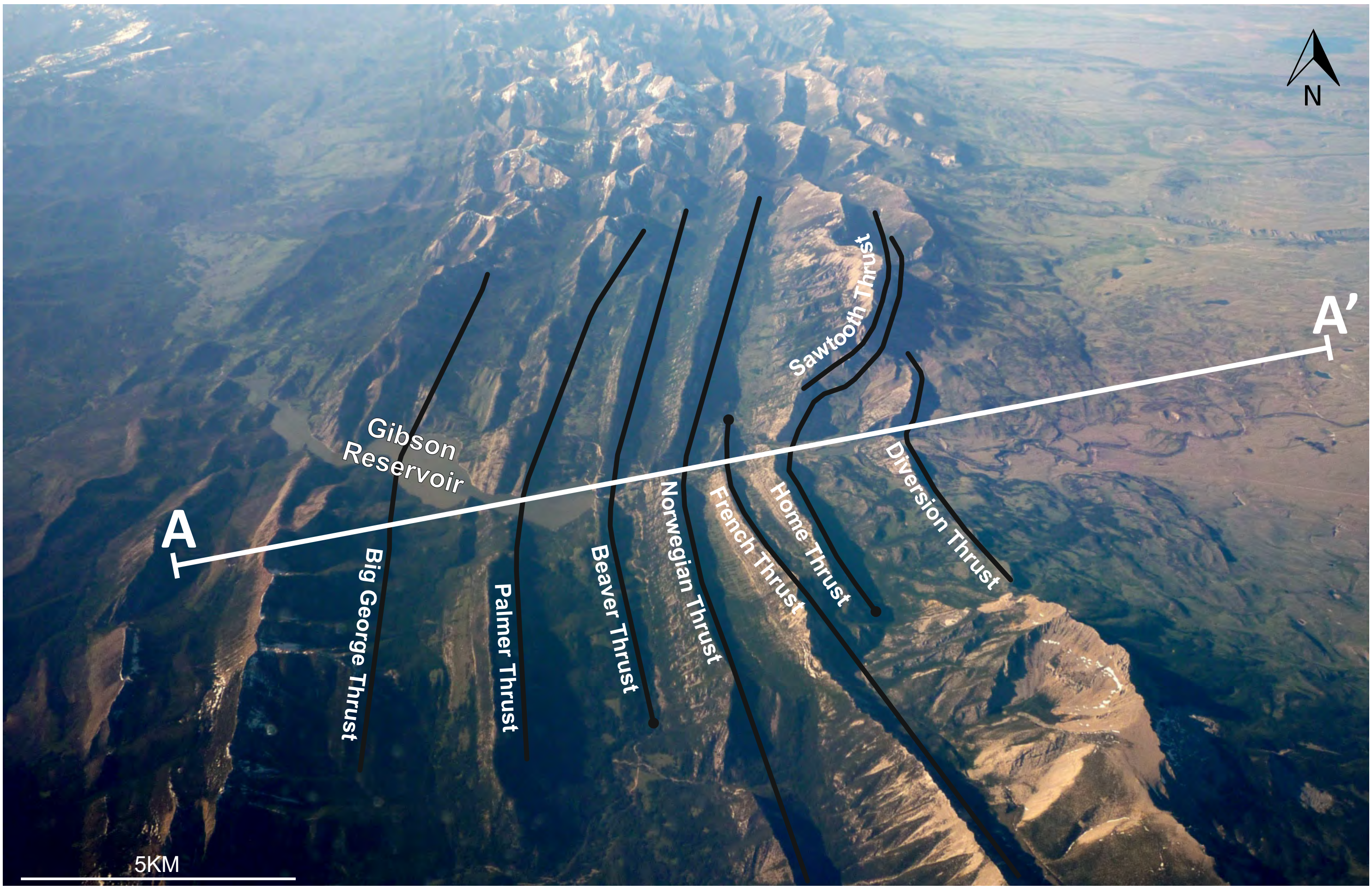
N
A
A’
Gibson Reservoir
Big George Thrust
Palmer Thrust
Beaver Thrust
Norwegian Thrust
French Thrust
Home Thrust
Sawtooth Thrust
Diversion Thrust
5KM

Figure 2

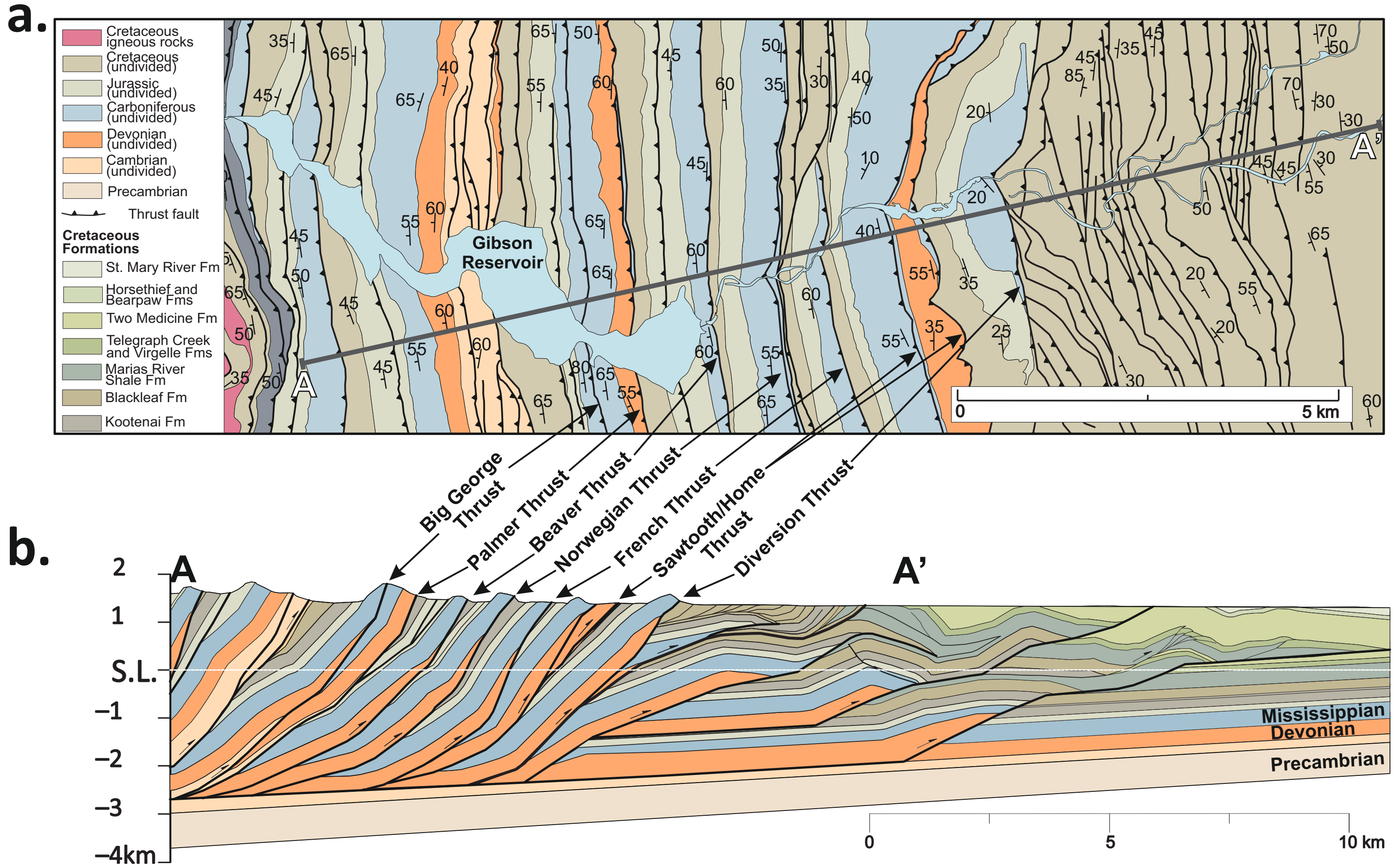

a.
Cretaceous igneous rocks
Cretaceous (undivided)
Jurassic (undivided)
Carboniferous (undivided)
Devonian (undivided)
Cambrian (undivided)
Precambrian
Thrust fault
Cretaceous Formations
St. Mary River Fm
Horsethief and Bearpaw Fms
Two Medicine Fm
Telegraph Creek and Virgelle Fms
Marias River Shale Fm
Blackleaf Fm
Kootenai Fm
Gibson Reservoir
A
A'
0
5 km
b.
Big George Thrust
Palmer Thrust
Beaver Thrust
Norwegian Thrust
French Thrust
Sawtooth/Home Thrust
Diversion Thrust
2
1
S.L.
−1
−2
−3
−4km
Mississippian
Devonian
Precambrian
0
5
10 km

Figure 3

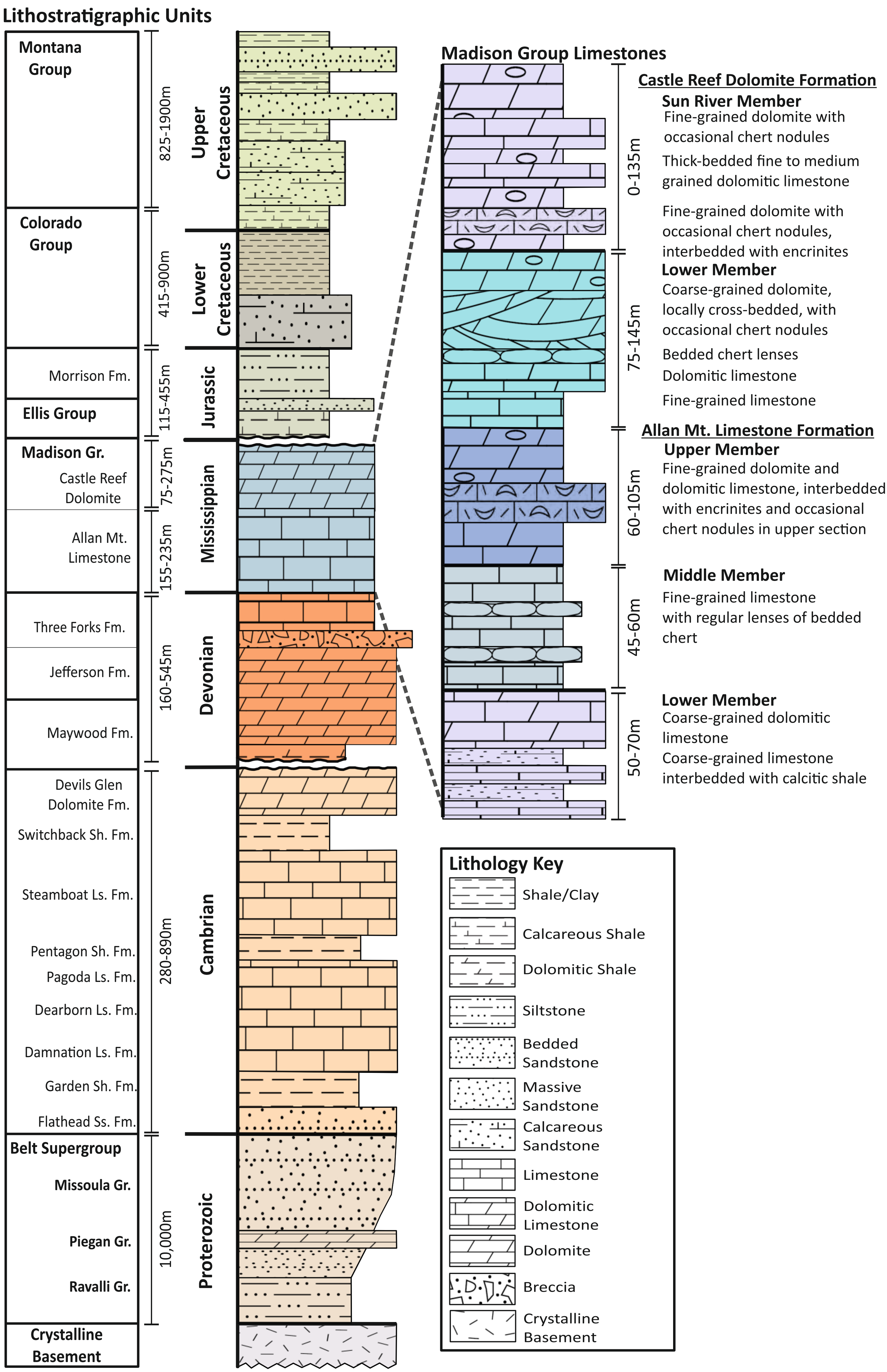
Lithostratigraphic Units
Montana Group
Colorado Group
Morrison Fm.
Ellis Group
Madison Gr.
Castle Reef Dolomite
Allan Mt. Limestone
Three Forks Fm.
Jefferson Fm.
Maywood Fm.
Devils Glen Dolomite Fm.
Switchback Sh. Fm.
Steamboat Ls. Fm.
Pentagon Sh. Fm.
Pagoda Ls. Fm.
Dearborn Ls. Fm.
Damnation Ls. Fm.
Garden Sh. Fm.
Flathead Ss. Fm.
Belt Supergroup
Missoula Gr.
Piegan Gr.
Ravalli Gr.
Crystalline Basement
825-1900m
415-900m
115-455m
75-275m
155-235m
160-545m
280-890m
10,000m
Upper Cretaceous
Lower Cretaceous
Jurassic
Mississippian
Devonian
Cambrian
Proterozoic
Madison Group Limestones
Castle Reef Dolomite Formation
Sun River Member
Fine-grained dolomite with occasional chert nodules
Thick-bedded fine to medium grained dolomitic limestone
Fine-grained dolomite with occasional chert nodules, interbedded with encrinites
Lower Member
Coarse-grained dolomite, locally cross-bedded, with occasional chert nodules
Bedded chert lenses
Dolomitic limestone
Fine-grained limestone
Allan Mt. Limestone Formation
Upper Member
Fine-grained dolomite and dolomitic limestone, interbedded with encrinites and occasional chert nodules in upper section
Middle Member
Fine-grained limestone with regular lenses of bedded chert
Lower Member
Coarse-grained dolomitic limestone
Coarse-grained limestone interbedded with calcitic shale
0-135m
75-145m
60-105m
45-60m
50-70m
Lithology Key
Shale/Clay
Calcareous Shale
Dolomitic Shale
Siltstone
Bedded Sandstone
Massive Sandstone
Calcareous Sandstone
Limestone
Dolomitic Limestone
Dolomite
Breccia
Crystalline Basement
Figure 4


W
E
Cretaceous
& Jurassic
Missisipian
Cretaceous
a.
W
E
b.
W
E
c.
S0
S1
d.
S1
e.
f.

Figure 5

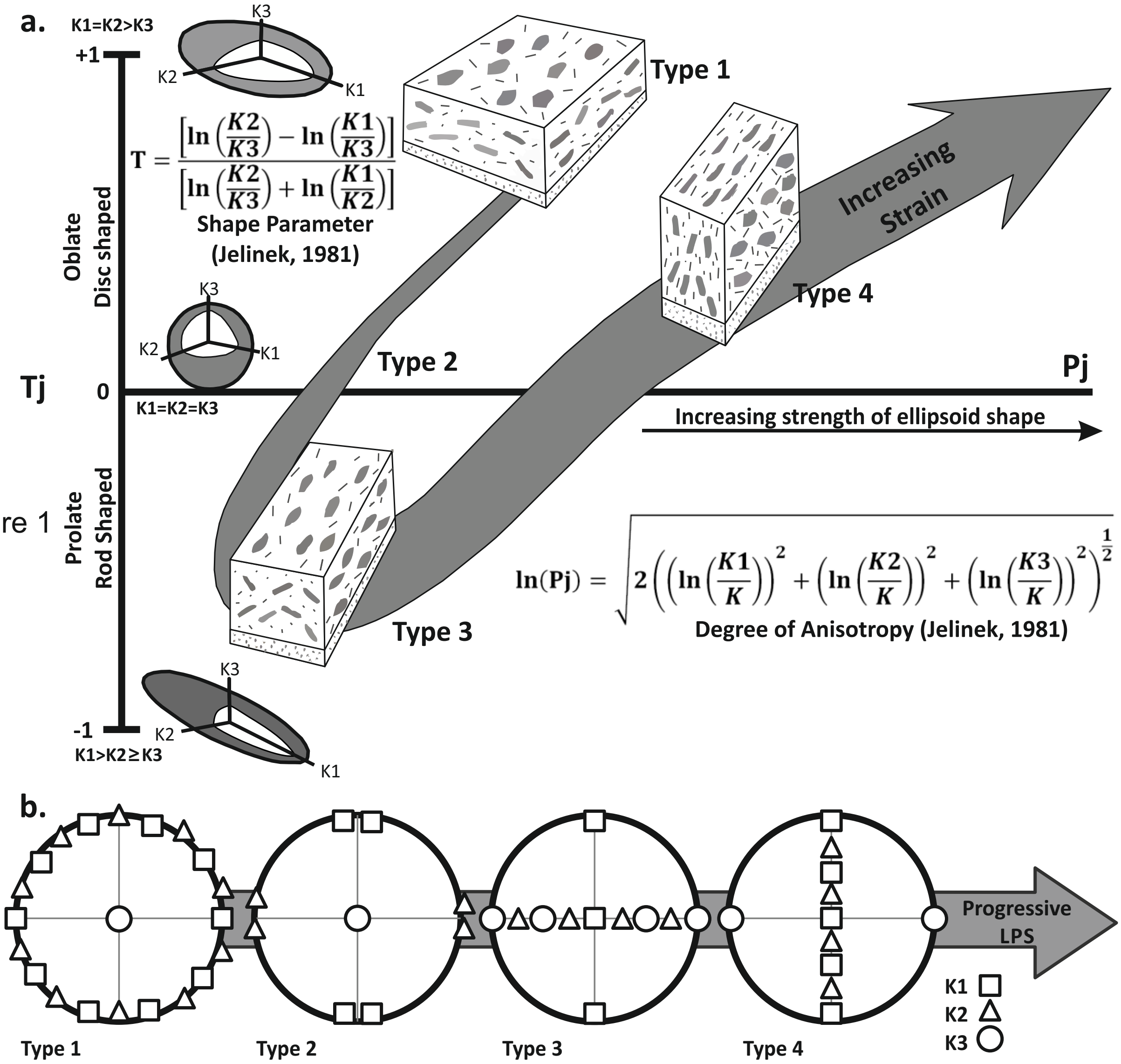

Figure 1

Figure 6

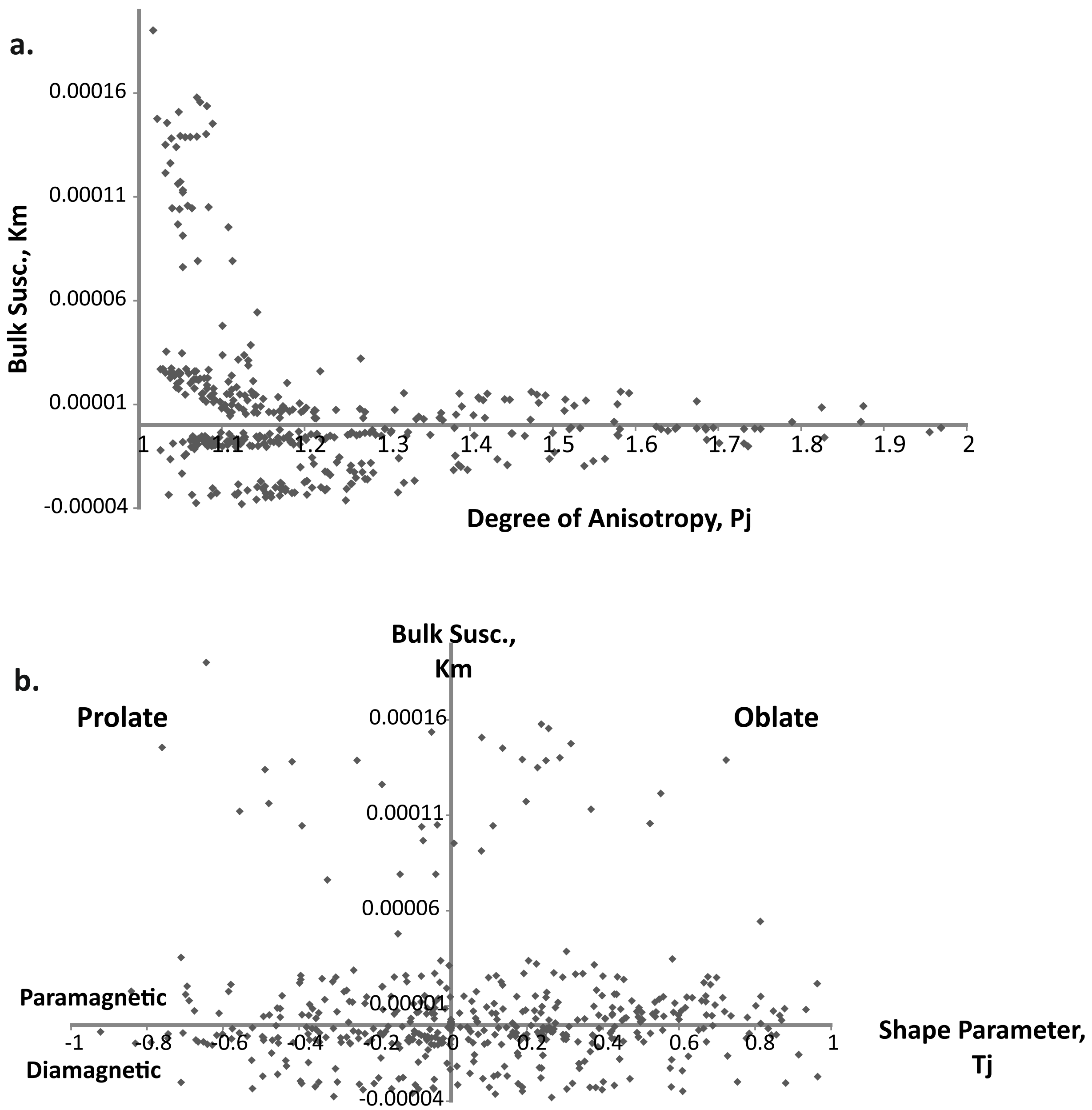
a.
0.00016
0.00011
0.00006
0.00001
-0.00004
Bulk Susc., Km
1
1.1
1.2
1.3
1.4
1.5
1.6
1.7
1.8
1.9
2
Degree of Anisotropy, Pj
b.
Bulk Susc., Km
Prolate
Oblate
0.00016
0.00011
0.00006
0.00001
-0.00004
Paramagnetic
Diamagnetic
-1
-0.8
-0.6
-0.4
-0.2
0
0.2
0.4
0.6
0.8
1
Shape Parameter, Tj

Figure 7

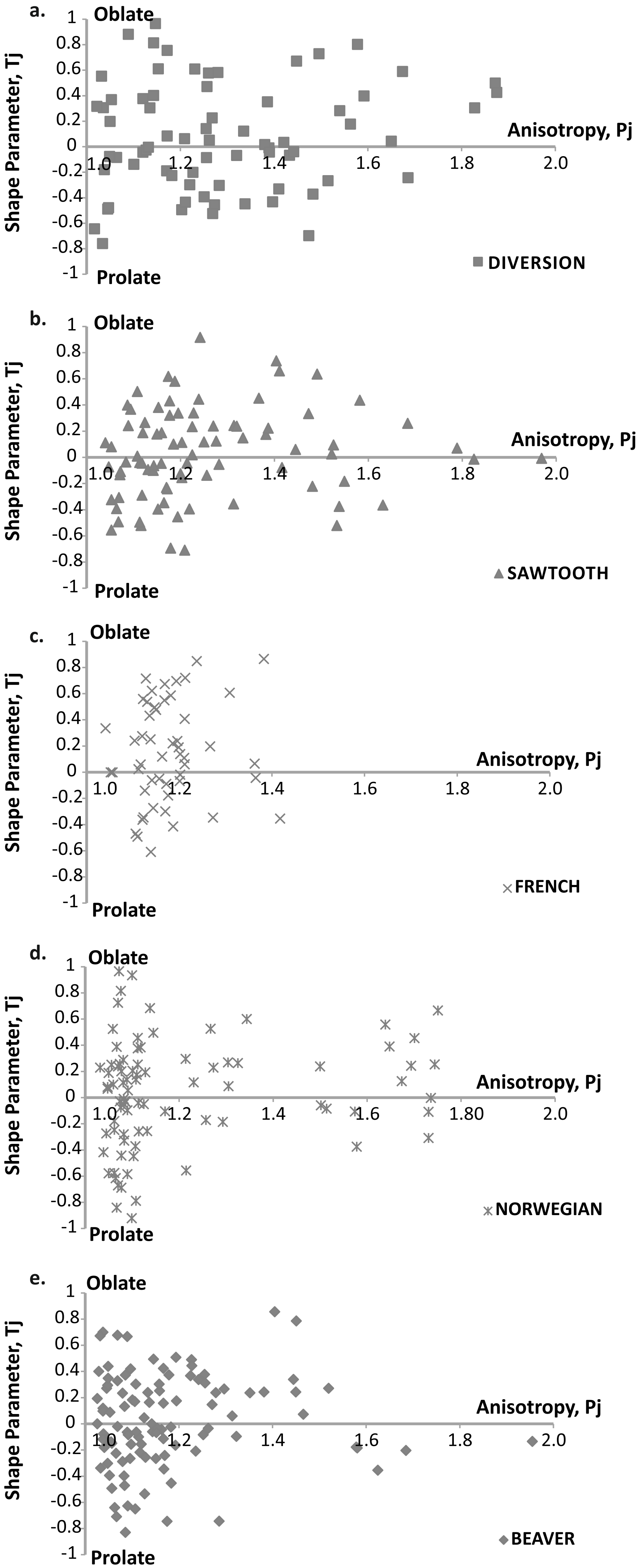
a.
Oblate
Shape Parameter, Tj
Anisotropy, Pj
Prolate
DIVERSION
b.
Oblate
Shape Parameter, Tj
Anisotropy, Pj
Prolate
SAWTOOTH
c.
Oblate
Shape Parameter, Tj
Anisotropy, Pj
Prolate
FRENCH
d.
Oblate
Shape Parameter, Tj
Anisotropy, Pj
Prolate
NORWEGIAN
e.
Oblate
Shape Parameter, Tj
Anisotropy, Pj
Prolate
BEAVER

Figure 8

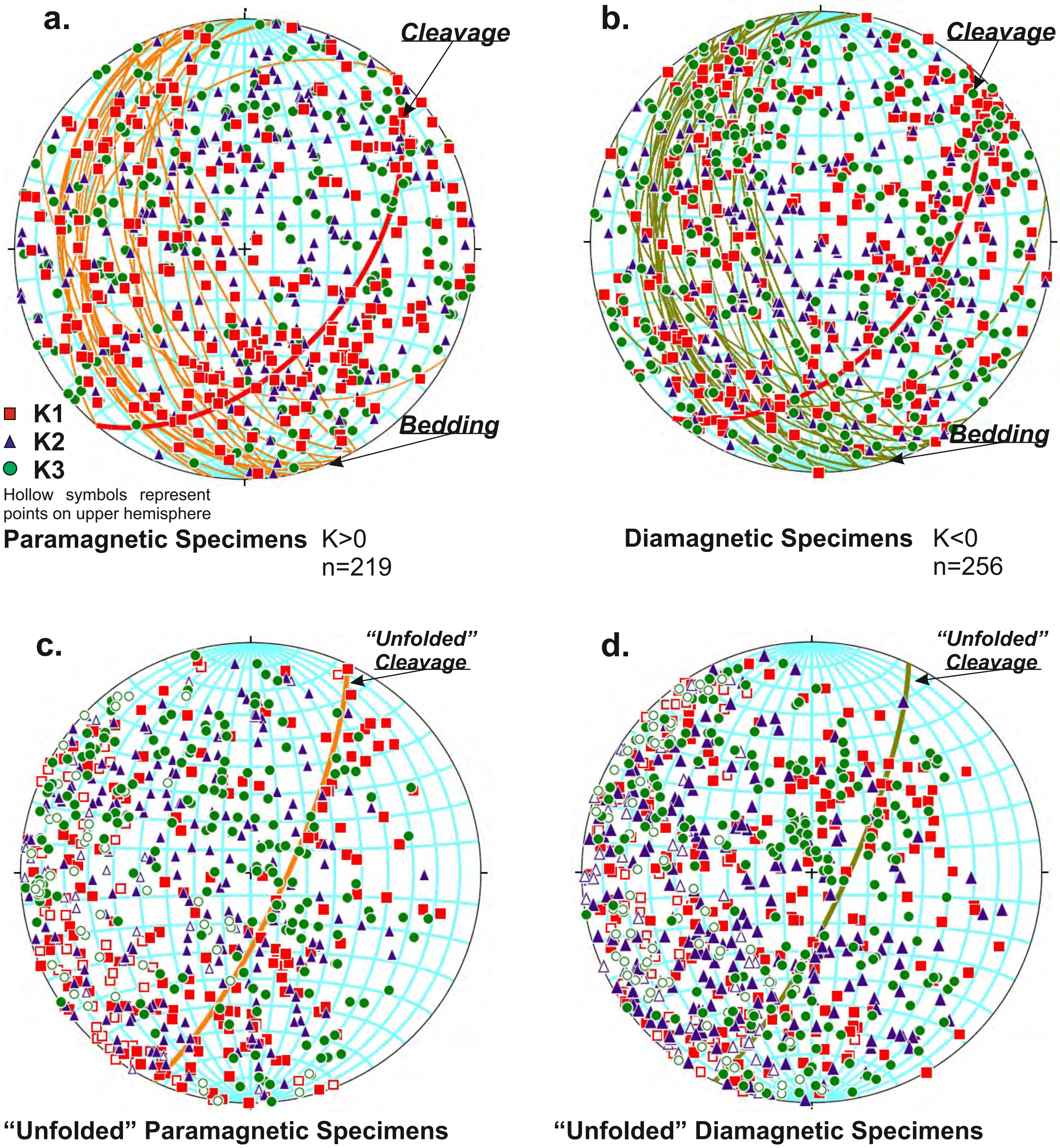
a.
Cleavage
Bedding
K1
K2
K3
Hollow symbols represent points on upper hemisphere
Paramagnetic Specimens K>0
n=219
b.
Cleavage
Bedding
Diamagnetic Specimens K<0
n=256
c.
"Unfolded" Cleavage
"Unfolded" Paramagnetic Specimens
d.
"Unfolded" Cleavage
"Unfolded" Diamagnetic Specimens

Figure 9

Figure 10

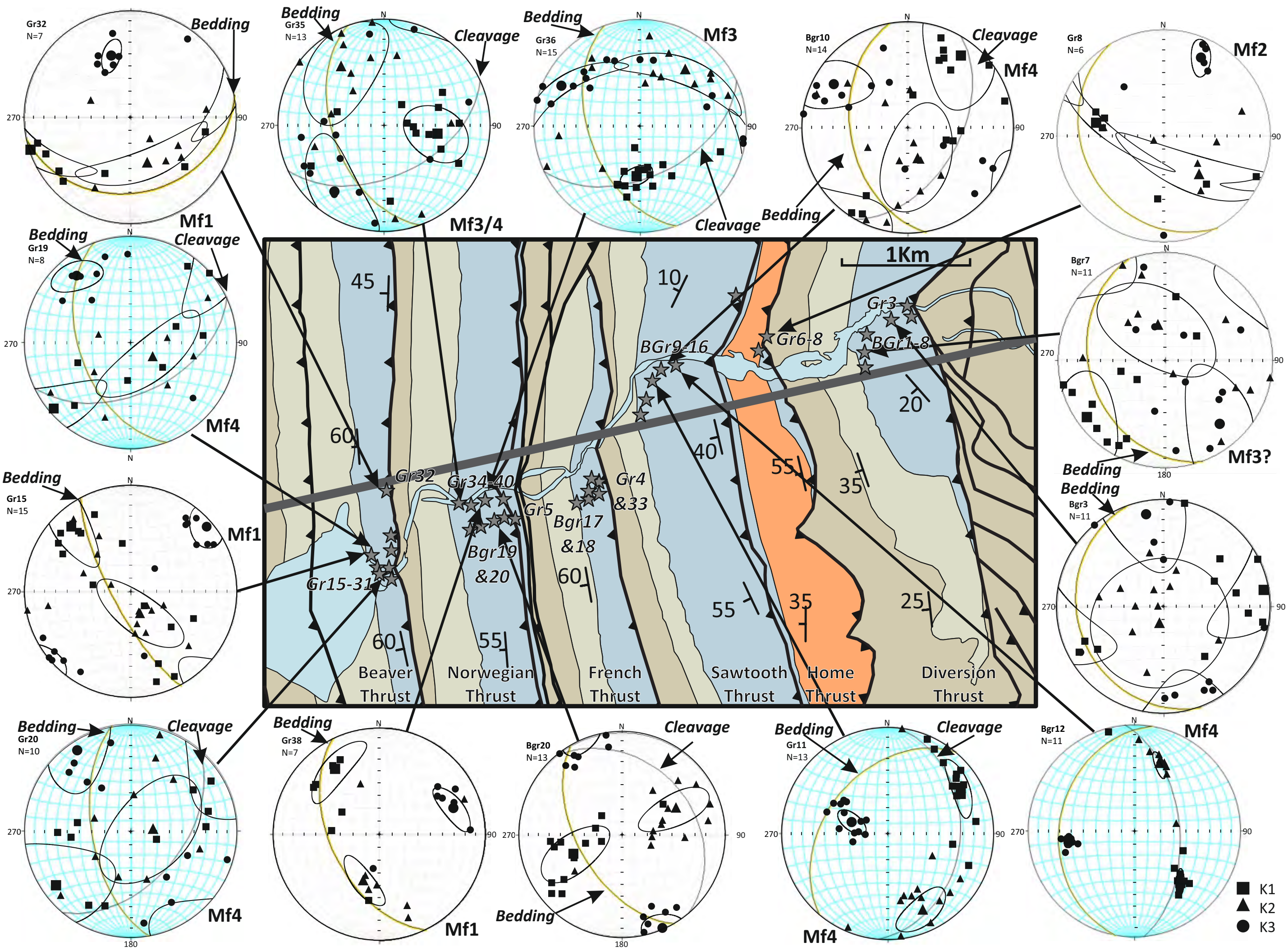
Beaver Thrust
Norwegian Thrust
French Thrust
Sawtooth Thrust
Home Thrust
Diversion Thrust
1Km
Gr32
Gr34-40
Gr5
Gr4 &33
Bgr17 &18
Bgr19 &20
Gr15-31
BGr9-16
Gr6-8
Gr3
BGr1-8
Bedding
Cleavage
Mf1
Mf2
Mf3
Mf3/4
Mf3?
Mf4
K1
K2
K3

Figure 11

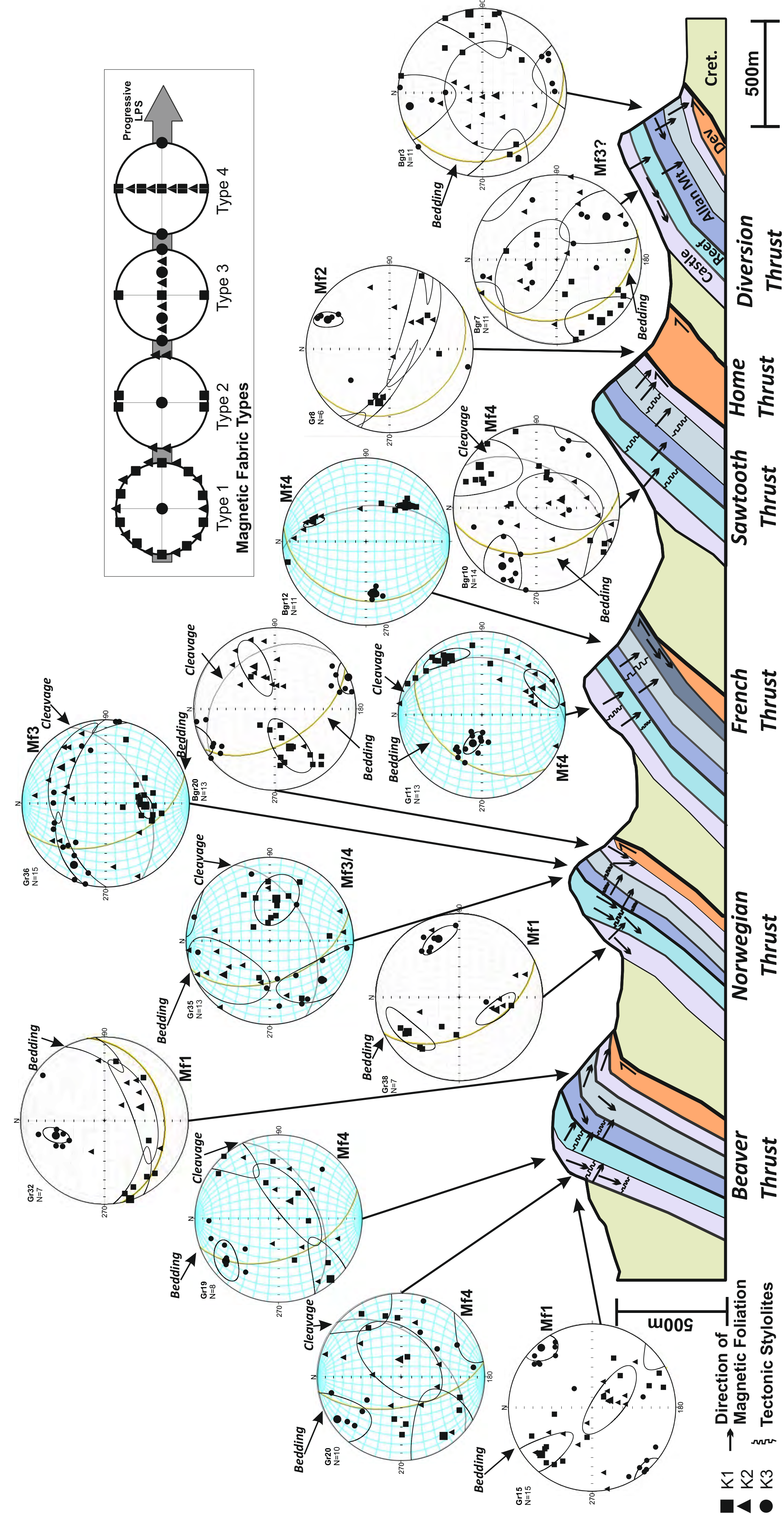

Progressive LPS
Type 1
Type 2
Type 3
Type 4
Magnetic Fabric Types
Cret.
500m
Dev
Allan Mt
Castle Reef
Diversion Thrust
Home Thrust
Sawtooth Thrust
French Thrust
Norwegian Thrust
Beaver Thrust
Mf1
Mf2
Mf3
Mf3/4
Mf4
Mf3?
Bedding
Cleavage
Gr15 N=15
Gr20 N=10
Gr19 N=8
Gr32 N=7
Gr35 N=13
Gr36 N=15
Gr38 N=7
Bgr20 N=13
Bgr12 N=11
Gr11 N=13
Gr8 N=6
Bgr10 N=14
Bgr7 N=11
Bgr3 N=11
K1
K2
K3
Direction of Magnetic Foliation
Tectonic Stylolites

Figure 12

a.

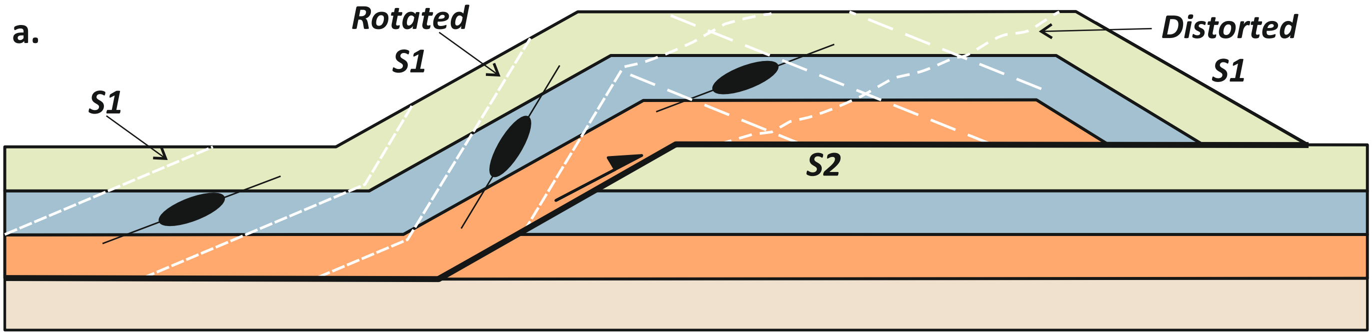

Rotated
S1
Distorted
S1
S1
S2

b.

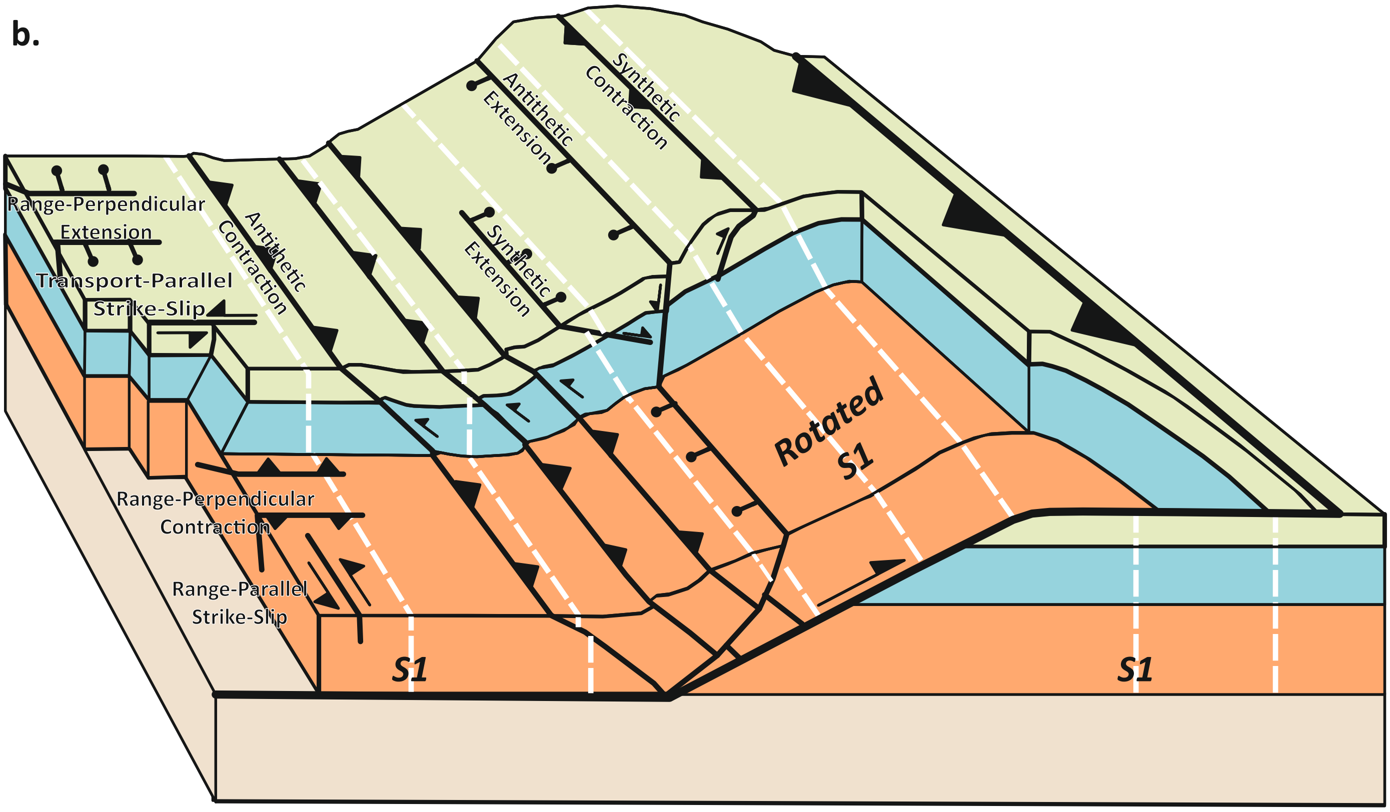

Synthetic
Contraction
Antithetic
Extension
Range-Perpendicular
Extension
Antithetic
Contraction
Synthetic
Extension
Transport-Parallel
Strike-Slip
Rotated
S1
Range-Perpendicular
Contraction
Range-Parallel
Strike-Slip
S1
S1